Quarterly Progress Report 3

Radar Studies of the Moon

15 August 1966

Issued 19 September 1966

Prepared for the U.S. National Aeronautics and Space Administration
under Contract NSR 22-009-106 by

Lincoln Laboratory

MASSACHUSETTS INSTITUTE OF TECHNOLOGY

Lexington, Massachusetts

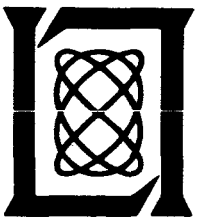

FOREWORD

The present report is the third in a series of quarterly progress reports called for under Contract NSR 22-009-106 between the National Aeronautics and Space Administration and Lincoln Laboratory, M.I.T. The first and the second of the quarterly progress reports will be referred to as QPR (1966:1) and QPR (1966:2) in the present report.

Section I of the present report describes the results of observations completed during the quarter from 1 May through 31 July 1966. This section is concerned with the observational results of an exhaustive study of the mean depolarizing properties of the lunar surface at 23 cm. It also contains the results of a determination of the angular scattering law of the moon at 3.8 cm, as well as the results of measuring the dependence of the scattering characteristics of the surface on the linear polarization of the scattering at that wavelength.

Section II contains information about work which was outlined in QPR (1966:1) and which is still in progress. This information relates in part to the progress of the mapping program at 3.8 cm and in part to the radar observations at 8 mm.

Section III discusses a method of observing the lunar surface whereby the ambiguity inherent in the range-Doppler mapping technique can be removed without relying on the resolution of the antenna beam.

AUTHOR

PRECEDING PAGE BLANK NOT FILMED.

CONTENTS

I. RESEARCH RESULTS

A. DEPOLARIZATION OF LUNAR RADAR ECHOES

1. Introduction

Several different experimental procedures are available for deriving different types of information about lunar surface properties. Measurements of the total lunar cross section have been carried out in the wavelength region from 8 mm to 22 m (Evans and Pettengill, 1963a; Davis and Rohlfs, 1964). Values of the cross section can be interpreted in terms of electrical properties of the surface material based on various models of the lunar surface. The most credible interpretations of the data at the moment appear to indicate that the dielectric constant of the surface material for wavelengths of a few decimeters is about 2.6 to 2.7 (Evans and Hagfors, 1964; Rea, et al., 1964). These estimates are based on the assumption that the lunar surface is homogeneous with depth and that an abrupt transition from vacuum to a dielectric medium takes place at the interface.

Measurements of the delay spread of the lunar echoes have been used to derive the backscattering cross section per unit solid angle per unit surface area as a function of angle of incidence. The angular variation of this cross section has, in turn, been used to derive certain statistical properties of the slopes of the lunar surface (Hagfors, 1961; Daniels, 1963; Beckmann, 1965a). Although there is general agreement about the interpretation of the echoes for small angles of incidence, the interpretation for larger angles is at present a subject of dispute. Some authors maintain that the returns even at large angles of incidence can be described in the usual Kirchhoff approximation if proper allowance is made for the geometric shadowing of the surface (Beckmann and Klemperer, 1965; Beckmann, 1965b). Others maintain the view that the scattering at larger angles of incidence can best be thought of as returns from individual discrete scatterers of size comparable with the wavelength of observation (Evans and Pettengill, 1963b; Evans and Hagfors, 1966).

More refined observational techniques have been developed to discriminate between different areas on the moon (Pettengill and Henry, 1962). These methods have been used to study the reflectivity of many features on the lunar surface (Thompson, 1965). It has been found that many craters, particularly rayed or younger ones, exhibit enhanced reflectivity at oblique incidence.

Most radar observations of the moon are carried out with circular polarization at the transmitter and with the receiver adjusted for the orthogonal circularly polarized wave. Observations have also been made in which the same circular polarization is received as was transmitted. Since this component should contain no energy in the case of an ideal reflector, this component has been termed "depolarized" (Evans and Pettengill, 1963b). Extensive depolarization studies of this type have been carried out at 68- and 23-cm wavelength (Evans and Hagfors, 1966). The study of the depolarization of lunar echoes by means of circularly polarized waves, however, does not exhaust the possibilities for polarization observations. There are many other combinations of transmitting and receiving polarizations which may yield independent data on the scattering properties of the surface. Examples of such additional polarization studies have been

published previously (Hagfors, et al., 1965; Evans and Hagfors, 1966) in preliminary form [see also QPR (1966:1) and QPR (1966:2)]. The present theoretical understanding of scattering from rough surfaces does not appear to be sufficiently well developed for fully utilizing the more complete measurements of depolarization properties discussed in this report or for making further deductions about the physical state of the lunar surface material. It will be shown, however, that a number of physically plausible conclusions can indeed be drawn from the observational results – at least in an heuristic manner.

The following sections discuss the number of different measurements required for the complete electromagnetic determination of the statistical backscattering properties of the surface. Because of the statistical nature of the problem, the transmitted and received radiations are adequately described in terms of second-order moments of the transverse fields – or in terms of a Stokes vector. The lunar surface is characterized by quantities relating various second-order moments of the radiation transmitted to those received – or in terms of a Mueller matrix. Because the radar system used calls for certain capabilities not commonly found in radar systems, the equipment used is very briefly described in Sec. 3 below. Section 4 contains a number of observational results obtained from the Millstone Hill radar at a wavelength of 23 cm, and also some results of polarization observations with the Haystack radar at a wavelength of 3.8 cm. Section 5 discusses at some length the significance of the observational results in terms of various physical models of the lunar surface, and also in the light of observational material from experiments not involving radar observations.

2. Electromagnetic Description of Scattering Process

A partly polarized plane electromagnetic wave traveling along the positive z-direction may be represented as

$$\vec{E}(z,t) = \vec{E}_o(t)\, e^{i(\omega t - kz)} \tag{1}$$

where $\vec{E}_o(t)$ is a slowly varying time function. The vector $\vec{E}_o(t)$ may be decomposed along two orthogonal directions, both orthogonal to the direction of propagation of the wave. The components along these directions, represented by unit vectors $\vec{e}_1$ and $\vec{e}_2$, will in general be complex phasors. When the field is a Gaussian process, every statistical property of the field may be found from the second-order moments of the various phasor components. If $\vec{e}_1$ and $\vec{e}_2$ correspond to the x- and y-directions, respectively, the field is thus completely specified by

$$\langle |E_x|^2 \rangle \quad , \quad \langle |E_y|^2 \rangle \quad , \quad \langle E_x E_y^* \rangle \quad \text{and} \quad \langle E_y E_x^* \rangle \quad .$$

The usual Stokes vector representation involves the following four linearly independent combinations of these moments:

$$\begin{aligned} S_1 &= \langle |E_x|^2 + |E_y|^2 \rangle \\ S_2 &= \langle |E_x|^2 - |E_y|^2 \rangle \\ S_3 &= \langle E_x E_y^* + E_y E_x^* \rangle \\ S_4 &= i \langle E_x E_y^* - E_y^* E_x^* \rangle \quad . \end{aligned} \tag{2}$$

Physically, S_1 is proportional to the total power in the wave, S_2 is the excess of power in the linear polarization along the x-direction over that in the y-direction, S_3 is the equivalent of S_2 with the references axes rotated through 45° in the positive direction and, finally, S_4 is the excess of the right circularly polarized power over that in the left.

The degree of polarization p is related to the extent to which the power in the wave can be separated into a single polarization. Numerically, the degree of polarization is equal to the maximum of the ratio of the difference between the power in two orthogonal modes and the total power in the wave. Appendix A briefly shows that the degree of polarization according to this definition is given by

$$p = \frac{1}{S_1}\sqrt{S_2^2 + S_3^2 + S_4^2} \tag{3}$$

which is also the usual definition (Born and Wolf, 1959, p. 551).

The wave in passing through a medium, and in being reflected or scattered from an interface will change its state of polarization, and hence the various components of a Stokes vector will be transformed. Such transformations may or may not alter the degree of polarization p.

The transformation of the four components of a Stokes vector, when the wave passes through a medium or is being scattered or reflected by a surface, may be described by a matrix M relating the Stokes vector before transformation $\vec{S}$ to that after transformation $\vec{S'}$, that is,

$$\vec{S'} = M\vec{S} \quad . \tag{4}$$

In the most general situation, the matrix M (the Mueller matrix) will contain 16 elements. In principle, therefore, we are required to determine from observations these 16 elements as a function of angle of incidence in order to achieve a complete statistical description of the scattering properties of the lunar surface. In the following paragraphs, we shall employ symmetry arguments and reciprocity relations to reduce considerably the number of unknowns to be determined experimentally in the case of lunar scattering.

Let us first perform a number of "Gedankenexperimente" to make use of symmetry properties. Suppose that the lunar surface is illuminated either with a right or a left circularly polarized wave, that is, $S = \{1, 0, 0, \pm 1\}$. Since we must expect the scattered power as well as the excess of linear polarization to be the same in the two situations, we have

$$\begin{aligned} M_{11} + M_{14} &= M_{11} - M_{14} \qquad \text{i.e.,} \qquad M_{14} = 0 \\ M_{21} + M_{24} &= M_{21} - M_{24} \qquad \text{i.e.,} \qquad M_{24} = 0 \\ M_{31} + M_{34} &= M_{31} - M_{34} \qquad \text{i.e.,} \qquad M_{24} = 0 \quad . \end{aligned} \tag{5}$$

Furthermore, the amount of "circular depolarization" must be the same in the two cases. This means that

$$M_{41} + M_{44} = -(M_{41} - M_{44}) \quad \text{i.e.,} \quad M_{41} = 0 \quad . \tag{6}$$

Reciprocity relations (Rumsey, 1954) also indicate that the power received in the y-component when transmitting waves are linearly polarized along the x-direction is the same as the power received in the x-component when the same transmitted wave is polarized along the y-direction. This must apply for arbitrary choice of x- and y-directions, which means that

$$M_{11} + M_{12} - M_{21} - M_{22} = M_{12} = M_{12} + M_{21} - M_{22} \qquad \text{i.e.,} \qquad M_{12} = M_{21}$$

$$M_{11} + M_{13} - M_{31} - M_{33} = M_{11} - M_{13} + M_{31} - M_{33} \qquad \text{i.e.,} \qquad M_{13} = M_{31} \quad . \tag{7}$$

Illumination of the moon with a linearly polarized wave cannot give rise to preferential circular polarization; hence, one must have

$$M_{42} = M_{43} = 0 \quad . \tag{8}$$

To proceed further with these arguments, we next orient the xy reference coordinate system with respect to the plane of incidence of the backscattering surface in such a way that the x-axis is in the plane of incidence. The Mueller matrix corresponding to this situation is denoted by M^o and its elements by M^o_{ij}.

In this situation, we might argue that the same total power must be scattered back irrespective of whether the transmitted linear polarization makes an angle of +45° or −45° with respect to the plane of incidence. This means that

$$M^o_{13} = M^o_{31} = 0 \quad . \tag{9}$$

The same two types of transmissions must give rise to identical values of S'_2, which means that

$$M^o_{23} = 0 \quad . \tag{10}$$

Transmission polarized linearly either in or across the plane of incidence for reasons of symmetry must give $S'_3 = 0$, which means that

$$M^o_{32} = 0 \quad . \tag{11}$$

For this particular choice of coordinate axes with respect to a scattering element, one therefore obtains, for M^o,

$$M^o = \begin{Bmatrix} M^o_{11} & M^o_{12} & 0 & 0 \\ M^o_{12} & M^o_{22} & 0 & 0 \\ 0 & 0 & M^o_{33} & 0 \\ 0 & 0 & 0 & M^o_{44} \end{Bmatrix} . \tag{12}$$

The matrix elements for other orientations of the coordinate axes can be found from Eq. (12) by a simple coordinate rotation transformation (see Appendix B). In particular, we see from Eq. (B-5) that the average of M over angle ψ is

$$\langle M \rangle_{\psi} = \begin{Bmatrix} M_{11}^{o} & 0 & 0 & 0 \\ 0 & \frac{1}{2}(M_{22}^{o} + M_{33}^{o}) & 0 & 0 \\ 0 & 0 & \frac{1}{2}(M_{22}^{o} + M_{33}^{o}) & 0 \\ 0 & 0 & 0 & M_{44}^{o} \end{Bmatrix} . \qquad (13)$$

Hence, it may be concluded that a complete statistical description of the electromagnetic backscattering properties of the lunar surface at each frequency and angle of incidence requires the determination of five independent quantities.

3. Experimental Equipment

The antenna beam of the Millstone Hill radar system is somewhat wider than the angular extent of the moon. Resolution in range discriminates between areas of constant angle of incidence. In order to separate small areas with a well-defined direction of the plane of incidence as seen from the radar system, additional discrimination had to be achieved by Doppler resolution. Because of a slight apparent angular rotation of the moon as seen from the radar, different areas on the moon will have different Doppler offsets with respect to that of the center of the lunar disk. Lines of constant Doppler offset will be straight parallel lines across the disk of the moon. Regions with near-zero Doppler offset correspond to areas where the local plane of incidence is nearly parallel to lines of constant Doppler offset. Areas of maximum Doppler offset for a particular range ring, on the other hand, have their local plane of incidence normal to lines of constant Doppler shift. For zero and maximum Doppler offset, therefore, the local plane of incidence of the area under study requires a well-defined direction with respect to the radar system. Range-Doppler cells with intermediate Doppler values correspond to a superposition of two areas on the moon with differently oriented planes of incidence, and therefore cannot be so conveniently employed in polarization studies.

Since the Doppler axis is rotating quite rapidly with respect to the radar system even on an hourly basis, it follows that polarization studies based on resolution by means of the range-Doppler technique can be carried out only if the feed polarization of the transmitting and receiving antennas can be adjusted rather freely and rapidly. Therefore, certain modifications had to be made to the original Millstone monopulse tracking feed system to meet these requirements.

The original feed system could be excited in the right or the left circularly polarized modes by applying the transmitter power to one or the other of two input ports to the feed system. In order to produce an arbitrary polarization of the transmitted wave, the power must be divided at will between these two ports and the relative phase of the two signals must be adjustable. The arrangement is shown schematically in Fig. 1. Phase changer Ph 2 controls the relative levels of the power at the input of the two antenna ports; phase changer Ph 1 controls their relative phase. For circular polarization, all the power is applied to one of the two antennas input ports; for linear polarization, the power is divided equally between the two antenna ports by adjusting Ph 2. The plane of linear polarization is then set by adjusting Ph 1. Arbitrary

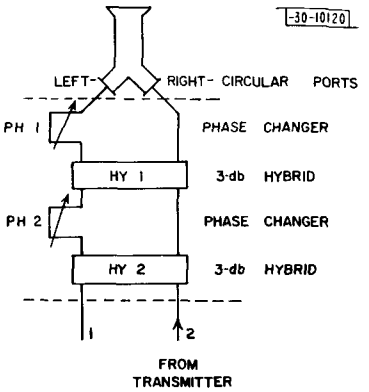

Fig. 1. Arrangement for control of polarization of transmitted radiation.

elliptical polarizations can also be produced, but were never used in the experiments described herein. All the adjustments described can be carried out during normal transmission conditions.

The modes of polarization received were controlled by an arrangement of phase changers and power splitters (hybrids) similar to that shown between the dashed lines in Fig. 1. The input to the arrangement was derived from ports 1 and 2 of Fig. 1. The receiver polarizations could, in principle, also be set up in the data-processing procedure by properly combining the four coherently detected quadrature components of the two polarizations. This requires the radio frequency amplifiers, as well as the various mixers and intermediate frequency amplifiers, to be stable in gain and phase, and tests on the existing equipment showed that this was not the case to the degree of accuracy required. By combining the two orthogonal received polarizations at radio frequencies – before passing the signal through any phase or gain sensitive components – the two receiver chains act essentially only as power measuring devices.

The degree of circularity transmitted could be checked by rotating a linear receiving dipole on the center of the antenna beam a distance of 500 m from the antenna. The ratio of maximum-to-minimum-power received on the linear dipole was about 0.3 to 0.4 db. When setting the system up for linear polarization, the maximum-to-minimum could easily be improved over 30 db. However, tests of the antenna in the receive mode showed that the two nominally orthogonal polarizations for some settings deviated from orthogonality by up to 5°. This, in turn, means that depolarization ratios smaller than some –18 db could not be measured.

The Haystack radar used to obtain some of the data reported below at a wavelength of 3.8 cm is at the moment equipped only to transmit a circularly polarized wave. The insertion of a network similar to that shown in Fig. 1, however, made it possible to receive either circularly polarized waves or an arbitrary pair of orthogonal linearly polarized waves.

4. Observations and Results

In this section, the observational techniques and results are briefly described. The various types of observations are related to the matrix elements of Eq. (12) in order to ensure that a complete electromagnetic description of the scattering is achieved. The observations are described in terms of increasing complexity beginning with incoherent results, i.e., results where all the power from a complete ring of constant range is combined. Thereafter, some observations are described in which the polarization of the receiving equipment is continuously changed to relate the receiver polarization to the Doppler cells on the moon. Finally, an

experiment is described in which both transmitting and receiving polarizations had to be changed continuously and independently in relation to lunar Doppler cells.

a. Measurement of Circular Depolarization, Range Ring Resolution Only

Measurements of circular depolarization have been carried out previously and have been reported elsewhere [QPR (1966:2)]; nevertheless, the main results are included briefly here for the sake of completeness.

Figure 2 shows the expected and the depolarized backscattered power plotted as a function of $\cos\varphi$, where φ is the angle of incidence. Both components have been corrected to account for the effect of the finite width of the polar diagram of the antenna. The two-way correction factor in decibels is plotted against $\cos\varphi$ in Fig. 3. The relative gain of the two orthogonal channels was checked by using a linearly polarized target transmitter and also by operating the radar system in a receiver mode as a radiometer with the moon as a thermal source. The two power gains were measured to be the same to within 10 percent. By gain ratio, we here refer to the ratio of powers received in the two orthogonal modes at the point where the noise calibration pulse is inserted into the system when the antenna is illuminated by a plane unpolarized wave along the main beam.

The ratio of the polarized and the depolarized components is plotted against $\cos\varphi$ in Fig. 4. Knowing the total relative power as a function of range, the ratio of the depolarized and the polarized components and the cross section of the moon measured with the polarized component only (Evans and Hagfors, 1966) suffices to determine the Mueller matrix elements M_{11}^{o} and M_{44}^{o} [see Eq. (12)]. We shall return to actual numerical evaluations and discussions of possible models in Sec. A-5, below.

b. Measurement of Linear Depolarization, Range Ring Resolution Only

The linear depolarization measurements were carried out by transmitting with a fixed (usually vertical) polarization. In order to avoid difficulties with Faraday rotation, the linear polarization at the receiver was rotated between runs. The output power in each polarization would therefore vary sinusoidally about a mean level proportional to $\frac{1}{2}M_{11}^{o}$ and with an amplitude proportional to $\frac{1}{4}(M_{22}^{o} + M_{33}^{o})$ [see Eq. (13)]. The least-mean-square sine-wave was fitted to the data and both the mean and depth of modulation were determined to give the total power and the power ratios. A correction for the polar diagram was made here as in the case of circular polarization (see Fig. 3). Figure 5 shows the polarized and the depolarized linear components plotted against $\cos\varphi$. Figure 6 displays the ratio of polarized to depolarized components again as a function of $\cos\varphi$. A comparison of these results with circularly polarized waves is presented in Sec. A-5, below. We only note here that this experiment, in addition to a redetermination of M_{11}, provides direct information about the quantity $M_{22}^{o} + M_{33}^{o}$.

c. Measurement of Power in Orthogonal Linear Polarizations for Circularly Polarized Illumination, Area Element Resolution

From Eqs. (12) and (13), it can be seen that the quantity M_{12}^{o} can only be determined provided resolution is available in addition to that provided by range gating, which was used exclusively in Secs. A-4-a and b, above. In order to determine M_{12}^{o} or the difference of the backscattering coefficients for waves polarized in and across the local plane of incidence, the moon

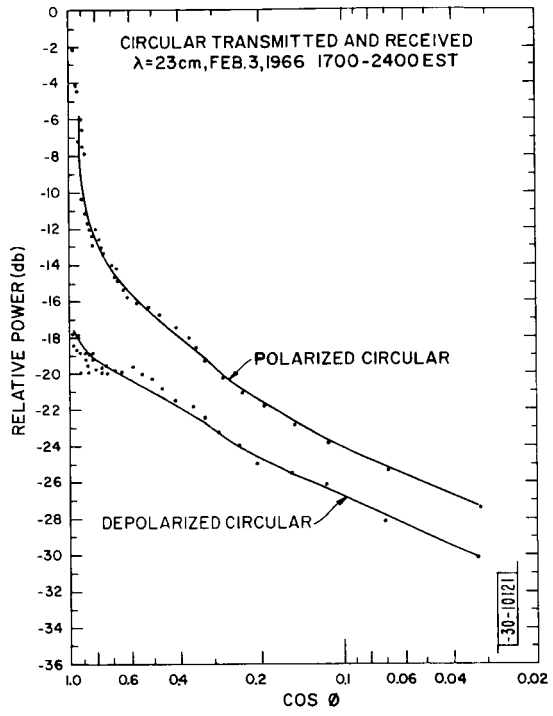

Fig. 2. Plot of polarized and depolarized circular components for circular polarization transmitted; relative power vs cosϕ (ϕ = angle of incidence).

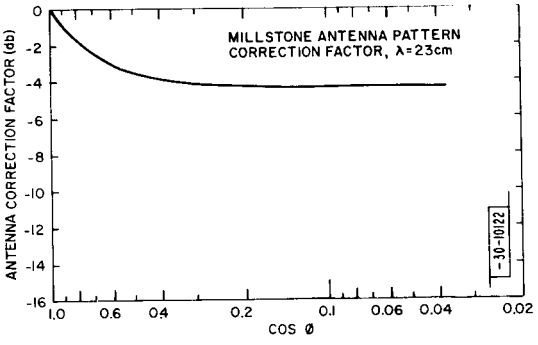

Fig. 3. Two-way antenna correction factor plotted vs cosϕ.

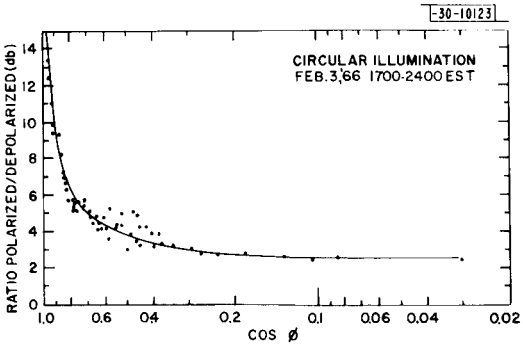

Fig. 4. Ratio of polarized and depolarized components vs cosϕ, circular polarization.

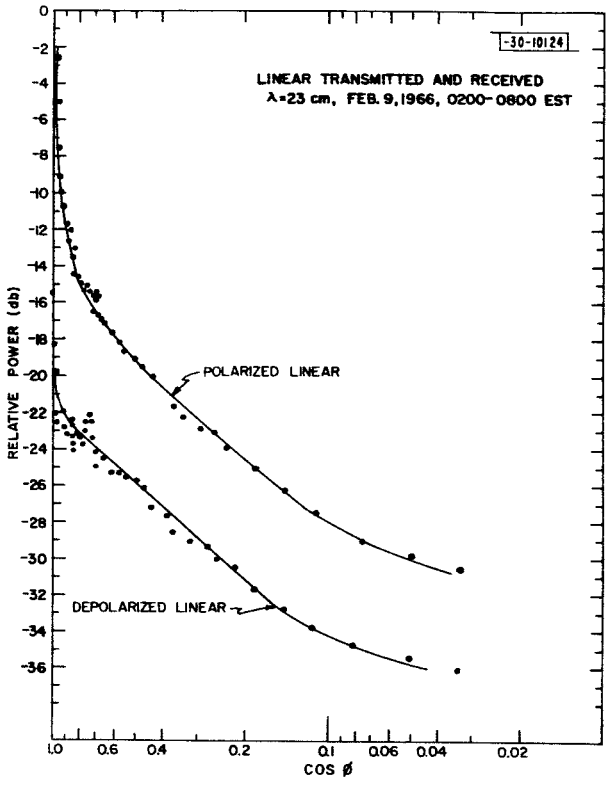

Fig. 5. Plot of polarized and depolarized components vs cos φ for linearly polarized illumination.

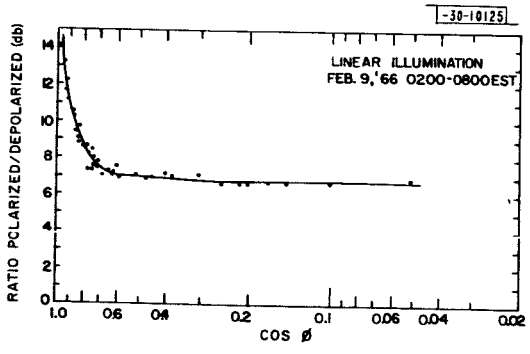

Fig. 6. Ratio of polarized and depolarized components vs cosφ, linear polarization.

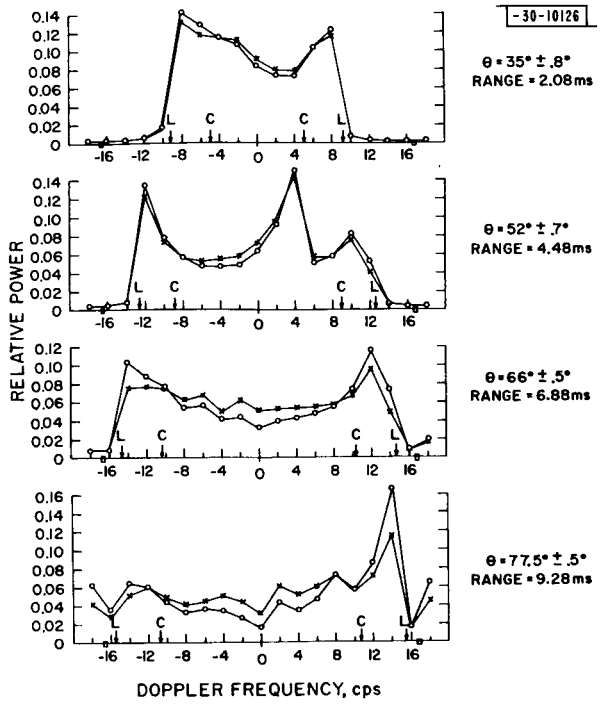

Fig. 7. Frequency spectra for two linearly polarized receiver components for circularly polarized illumination.

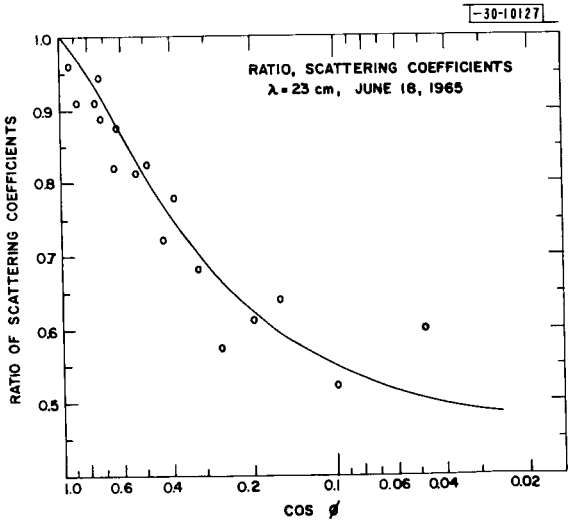

Fig. 8. Ratio of backscattered power in two orthogonal linearly polarized components for circularly polarized illumination.

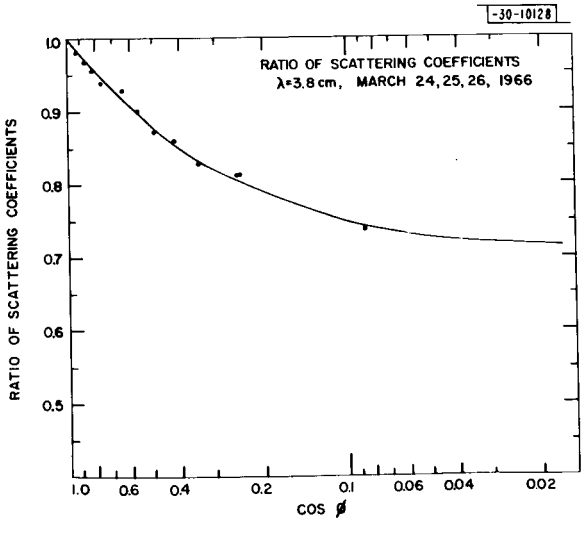

Fig. 9. Ratio of backscattered power in two orthogonal linearly polarized components for circularly polarized illumination, at 3.8-cm wavelength.

was illuminated by a circularly polarized wave and the two receiver chains were adjusted so that one was sensitive to linearly polarized waves with direction of polarization parallel to the projected libration axis of the moon and the other was perpendicular to this axis. Any variation in the backscattering coefficient with the angle measured with respect to the local plane of incidence must show up as a difference in the frequency spectrum of the return for a particular range ring on the moon. For a more detailed description of the basic principles involved in this experiment, the reader is referred to Hagfors, et al. (1965). Figure 7 shows a few normalized spectra for the two receiver polarizations. The normalization consists in forcing the two frequency spectra corresponding to the same range to have the same area, i.e., the same returned power. As can be seen, the component corresponding to E-field aligned with the libration axis is stronger than the other near-zero frequency, but is less strong than the other near-maximum frequency for the range ring considered. The effect observed could, in principle, be obtained if the antenna beam for the two linear polarizations were different. Scans of the solar disk with the receivers used as radiometers were therefore made for both linear polarizations, the scans being carried out both in azimuth and elevation. These tests showed that the polar diagrams were identical to within 5 percent at an angular separation from the center of the beam corresponding to the limb of the moon.

The ratio of the two backscattering coefficients was derived from curves such as those shown in Fig. 7 and the ratio plotted against $\cos\varphi$ in Fig. 8. This determines the matrix element M_{12}^{o} in Eq. (12). Note that the component which has its E-field in the local plane of incidence is the stronger one.

A series of lunar polarization experiments, similar to those described so far for a wavelength of 23 cm, have been initiated at a wavelength of 3.8 cm and the equivalent of the experiment described here has been carried out. In the 3.8-cm experiment using the Haystack antenna, the beamwidth is approximately only one-tenth of the diameter of the lunar disk. The angular resolution necessary to define a local plane of incidence on the moon is, therefore, provided directly by the beam itself and by a range resolution capability. In practice, the experiment was carried out by transmitting in the circularly polarized mode and by receiving two orthogonally polarized linear components. The antenna beam was moved out from the center of the lunar disk to the limb in steps along a radius of the disk, and the polarization of the receiver channels was adjusted so that one was aligned with the radius and the other was perpendicular to this radius. The center of the disk was used as a reference point where the backscattering coefficients for the two orthogonal polarizations by definition are equal. The results of the experiment are displayed in the form of a ratio of the power in the components polarized parallel and perpendicular to the local plane of incidence, and are shown in Fig. 9 on the same scale as in Fig. 8 for the 23-cm results.

d. Measurement of Power in Orthogonal Linear Polarizations for Linearly Polarized Illumination, Area Element Resolution

The three basic types of experiments discussed so far still leave one quantity in Eq. (12) undetermined. Only the sum of M_{22}^{o} and M_{33}^{o} is known, and it is necessary to determine one of the two elements by an additional experiment.

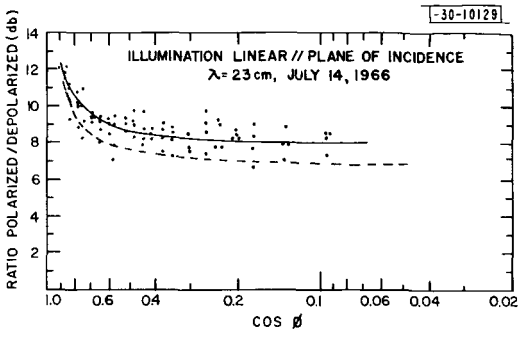

Fig. 10. Ratio of backscattered power in two orthogonal linearly polarized components for linearly polarized illumination, polarization || plane of incidence. Dashed curve shows depolarization when polarization of illumination is averaged over all angles – for same data.

The particular setup chosen to separate M_{22}^{o} and M_{33}^{o} in Eq. (12) consists in transmitting a linearly polarized wave in such a way that the direction of polarization is aligned with the direction of the instantaneous libration axis of the moon. The two orthogonally polarized receiver channels were aligned so that one corresponds to polarization in the local plane of incidence and the other is normal to this plane. The experiment was carried out both by making use of the rotation technique at the receiver and as described in Sec. A-4-b and by actually aligning the receiver polarizations under conditions of low Faraday rotation. The results are shown in Fig. 10 which displays the ratio of the two components as a function of $\cos\varphi$. The comparatively large spread in the observed values is not completely understood. The most likely explanation is presently thought to be that local variations exist in the scattering properties of the lunar surface. It should be noted, however, that the amount of depolarization is less from a Doppler strip than from a whole range ring when the illumination is linearly polarized parallel to this strip.

5. Discussion of Polarization Results

As was indicated in the previous sections, the polarizing or depolarizing ability of the lunar surface as a whole has been completely determined for backscattering at 23 cm and its study has begun at 3.8-cm wavelength. The extension of this program might consist in attempting to detect local variations in these properties over the surface. Such a program could be carried out quite readily provided sufficient beam resolution is available in the radar system to remove the ambiguity inherent in the range-Doppler observation technique [see QPR (1966:1), Sec. I-H]. This is the case at 3.8 cm where the Haystack antenna can be used. At 23 cm, however, the ambiguities cannot readily be removed by means of the polar diagram, and certain other methods are contemplated to achieve the same aim. These ideas are described briefly in Sec. III of the present report.

In order to place the measurements at 23 cm on an absolute basis, we first establish the backscattering cross section per unit area as a function of angle of incidence from the data supplied in QPR (1966:2). By using the cross section of 0.065 for the whole moon and the power-vs-range data of Fig. 2, the values of cross section in m^2 per unit surface area (also in m^2) were derived for a few representative delay values (see Table I).

TABLE I
BACKSCATTERING CROSS SECTION PER UNIT SURFACE AREA

Delay (msec)	Angle (deg)	Cross Section (db)
2	34	−15.2
3	42	−16.8
4	49	−18.0
5	55	−19.1
6	61	−20.2
7	67	−22.6
8	72	−23.2
9	77	−25.3
10	82	−27.9

Let us now turn to a somewhat qualitative discussion of a possible explanation for the various depolarization results presented above. A quantitative discussion will follow in a subsequent quarterly progress report. The scattering near normal angles of incidence was described in QPR (1966:1) and is adequately understood in terms of the quasi-specular scattering theory outlined there. The quasi-specular scattering theory, however, is inadequate when it comes to explaining the polarization effects observed at rather oblique angles of incidence. The reason for this is the method of establishing the boundary conditions in the Kirchhoff theory (Beckmann and Spizzichino, 1963). Since the boundary conditions are established locally by means of the tangential plane approximation, the appropriate reciprocity relations between transmitter and receiver will only hold, in general, for a perfectly conducting boundary. For an essentially dielectric boundary, the reciprocity relationships will only be satisfied as long as the scattering can be regarded as a superposition of contributions from specular points as in reflection from the region near normal angles of incidence, or in backscattering from a surface having large smooth areas with high slope angles.

When the angle of incidence is sufficiently large that the number of specular points becomes very small, one might expect small-scale undulations in the surface to become the dominant cause of the scattering. The Kirchhoff theory is not accurate enough to handle the scattering from small scales when the boundary is a dielectric, as pointed out above. However, perturbation methods have been worked out for this case and the results are available (Rice, 1951; Peake, 1959). This latter type of theory appears to be able to account for scattering comparable in strength to what is actually observed in the case of the lunar surface (see Table I). The theory also appears to predict that the scattering at oblique angles of incidence is stronger when the E-field is in the plane of incidence than when the E-field is perpendicular to this plane, although this ratio as predicted by the theory appears to be much smaller than what is actually observed (see Fig. 7 and compare Peake, 1959). The major deficiency of the theory when applied to lunar surface scattering, however, stems from its inability to predict a depolarization in the sense

of the results shown, particularly in Fig. 9. In other words, the perturbation theory predicts that for linearly polarized waves, with E-field either in or perpendicular to the local plane of incidence, all the energy should come back in the same polarization as that of the transmitter. We therefore, at least tentatively, are forced to reject the simple perturbation theory of backscattering of electromagnetic waves as a satisfactory explanation of lunar scattering.

It has also been suggested that many of the depolarization effects may be explained in terms of multiple scattering. Again, this appears very unlikely to us in view of the extremely low reflectivity of the lunar surface material. Multiple scattering should only contribute a very small fraction of the total backscattered energy and should not be strong enough to affect the depolarizing properties at all.

The depolarization of circularly polarized waves as observed in lunar echoes cannot be explained merely on the basis of a different backscattering coefficient for the two principal linear polarizations. The ratio of the two coefficients is never smaller than 0.5 (see Fig. 7). If this were the only cause of the depolarization of circularly polarized waves, the ratio of expected to depolarized returns should be about 15 db, and not about 2.5 db as is actually observed (see Fig. 4).

It therefore appears, at the present time, that the lunar echoes at oblique angles of incidence must be primarily caused by scattering from discrete scatterers which are asymmetric in such a way that the polarization of the backscattered radiation is not the same as that of the incident wave. These scatterers are probably identical to the rocks which can be seen strewn over the surface in the recent Surveyor I pictures.† In the preliminary report just referred to, the cumulative rock distribution was determined to be given by

$$N = 3 \cdot 10^{5} \cdot y^{-1.77} \tag{14}$$

where

N = cumulative number of grains per $100\,m^2$, and
y = diameter of grains in mm.

The number density of rocks or grains per m^2 with diameter between y and $y + dy$ is

$$n(y)\,dy = 5.31 \cdot 10^{3} \cdot y^{-2.77} \quad . \tag{15}$$

The geometric cross section of each grain expressed in m^2 is

$$\sigma_g = \frac{\pi}{4} y^2 \cdot 10^{-6} \quad . \tag{16}$$

Let each grain scatter back with a certain fraction R of its cross section when the diameter exceeds the wavelength of observation, and not scatter back at all when the wavelength is larger than the diameter. The cross section per unit area due to the rocks is therefore, at least in order of magnitude,

† See "Surveyor I, A Preliminary Report," Report SP-126, National Aeronautics and Space Administration (June 1966).

$$\sigma \approx R \cdot \frac{\pi}{4} \cdot 5.31 \cdot 10^{-3} \int_{y_{min}}^{y_{max}} y^{-0.77}\, dy = \frac{\pi R}{4} \cdot 5.31$$

$$\cdot\ 10^{-3}\ \frac{1}{0.23}\ (y_{max}^{0.23} - y_{min}^{0.23}) \quad . \tag{17}$$

The distribution Eq. (14) emphasizes larger rocks, i.e., the larger rocks obscure more of the surface area than do the smaller ones. For this reason, one must somewhat arbitrarily place an upper limit on y. The cross section σ is not very critically dependent upon this choice, however. Suppose we put $y_{max} = 23$ cm. Equation (17) then gives

$$\sigma \approx R \cdot 0.083 \quad . \tag{18}$$

If the reflectivity R of the grains is the same as for the moon as a whole, the cross section per unit area is

$$\sigma \approx -23\ \text{db} \quad . \tag{19}$$

A comparison with the data in Table I shows that the number of rocks may be adequate to account for the scattering. The calculation may have overestimated the cross section of the rocks somewhat, but probably only by a fraction of an order of magnitude. If the Flamsteed area where Surveyor I landed is typical of the lunar surface, it appears that the previous interpretation of radar data in terms of a layer covering up most of the scatterers (Hagfors, et al., 1965) is in difficulty. The Surveyor I data indicate that there is, on the average, at least one rock of diameter exceeding one meter per 100 m^2 of the surface. Our earlier interpretation of the radar polarization data rests on the assumption that such rocks are virtually absent on the surface. This assumption was made because of the apparent absence of positive relief features in the photographs obtained in the Ranger flights.

Further work to reconcile the radar data with the findings of the Surveyor I pictures is under way and will be presented in a future quarterly progress report. In particular, the angular dependence of the scattering, both polarized and depolarized, must be explained in detail; in fact, the depolarization of the linearly and circularly polarized waves must be explained in detail, as well as the difference between the two principal backscattering coefficients of the surface and the wavelength dependence of this difference.

B. DETERMINATION OF ANGULAR SCATTERING LAW FOR LUNAR SURFACE AT 3.8 cm

During the past year, the scattering behavior of the moon has been determined using our 23-cm Millstone radar. These measurements represent a small part of the work called for in our contract with NASA, and form the subject of the research results presented in QPR (1966:2). Measurements are now being undertaken at Haystack to examine the behavior at 3.8-cm wavelength.

The moon's scattering is known to change markedly as a function of wavelength. We think that this arises partly because the surface is covered with an increasing amount of small-scale structure, and hence appears "rougher" as the wavelength is reduced, and partly because the surface may be inhomogeneous so that different wavelengths penetrate to different depths [QPR (1966:1)].

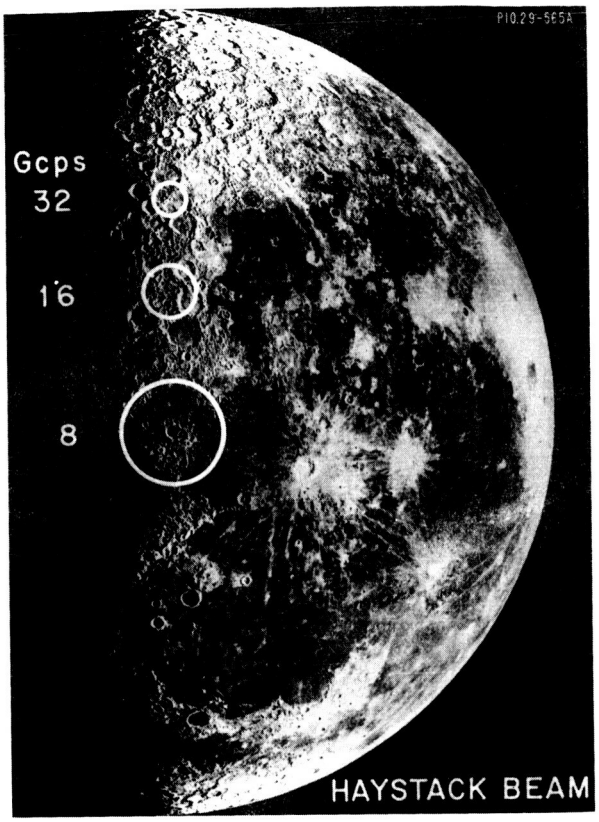

Fig. 11. Half-power beamwidth of Haystack antenna on surface of moon. For observations reported here at 3.8cm, largest (8-GHz) pattern is appropriate, except that in radar observations antenna weighting is imposed twice so that useful field of antenna is somewhat smaller than indicated.

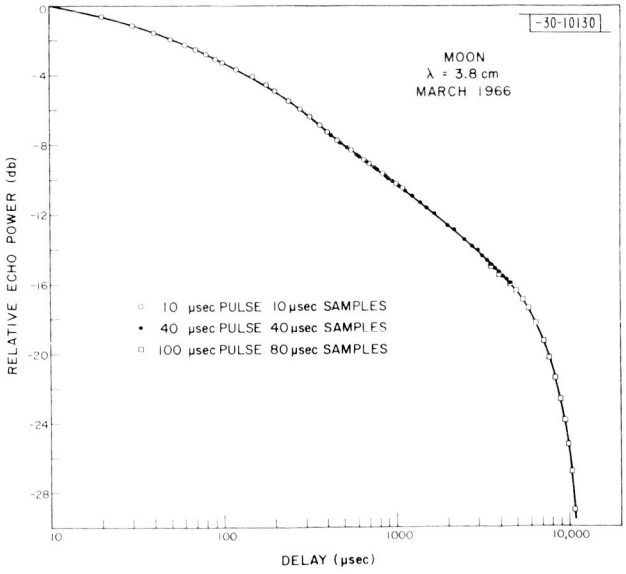

Fig. 12. Echo power vs delay law $\bar{P}(t)$ determined for 3.8-cm wavelength during observations described in text.

Previously, X-band observations were made of the moon in 1962 by Evans (1962) using the Camp Parks radar. It is now possible to secure more accurate results using the Haystack radar system because of the better pointing accuracy and superior signal-to-noise ratio which it provides and as a result of the better range tracking and integration techniques available with the Millstone Craig/Fleck machine and SDS 9300 computer combination.

Observations to determine the angular scattering law for the polarized or expected component of the echoes were made with Haystack for about 7 hours each morning from 16 to 19 March 1966. At Millstone, the antenna beam illuminates the whole moon so that the complete law for the variation of echo power in delay can be established with the beam directed at the moon's center. In practice, it is usually necessary to employ a variety of pulse lengths so that good delay resolution (using short pulses) can be obtained for the region around the subradar point, and yet good signal-to-noise ratio may be maintained for the limbs (using longer pulses). For these new observations, the same requirements hold but, in addition, the beam must be scanned off-center. Figure 11 illustrates the size of the Haystack antenna beam between 3-db points on the disk of the moon. For radar observations, the weighting imposed by the antenna beam occurs twice so that the effective beamwidth is of the order of 3 min. arc or one-tenth the angular diameter of the moon. In the measurements made in March 1966, a pulse of 10 μsec with a 10-μsec associated sample spacing was employed to explore the central region. Measurements were made for periods of 5 min. for beam positions of 0 to 5 min. with respect to the center in 1-min. steps. The beam was scanned away from the center in four mutually perpendicular directions. The region 6 to 12 min. was later explored in 1-min. steps using 40-μsec pulses and an associated 20-μsec sample interval. The beam was scanned away from the center in eight directions intersecting at 45° angles. Finally, the limb region 12 to 15 min. was explored in the same eight directions using a 100-μsec sample interval.

In all these observations, the antenna offsets from the moon's center were inserted manually. The timing of the Haystack radar was locked to that at Millstone so that the Millstone "range drifter" (Craig/Fleck machine) could be used to sample the echoes as in earlier 23-cm moon observations. The IF signal transmitted to Millstone via the intersite coupling was at 2 MHz so that adequate bandwidth (100 kHz) could be obtained for the 10-μsec-pulse measurements. The runs were processed at Millstone using the SDS 9300 computer to obtain the integrated echo power vs delay. The speed of this program is such that the data integration is completed shortly after the end of the operation.

Only one difficulty was encountered during these operations: the failure of the power amplifier pulse modulator to operate continuously above approximately 30-kv applied voltage. It was necessary to raise the voltage slowly during the first hour in order to reach 75-kw peak-power output. Even at this level, however, the modulator safety circuits would trip intermittently.

The data obtained in the manner described above have been analyzed to obtain the plot of echo power vs delay shown in Fig. 12. In order to obtain this plot, it was necessary to average all the echo-power-vs-delay plots obtained for a given antenna offset and then to correct this mean curve for the weighting imposed by the antenna beam. In this way, portions of the total curve were built up. A check on the accuracy of the procedure was afforded by a comparison

of the curves in the regions where they overlap. A change in the assumed beam shape was required before such consistency was achieved. The curve shown in Fig. 12 is in reasonable agreement with the earlier results, but provides better resolution for the region 10 to 200 μsec.

Table II lists the scattering laws obtained for the moon at λ = 3.8, 23, and 68 cm using Lincoln Laboratory radars. As the resolution in delay was the same in all three sets of measurements, these data accurately reflect the change in scattering behavior with wavelength.

The new results do not change any of the conclusions reached in QPR (1966:1) concerning the effective mean slope of the lunar surface at this wavelength. They do, however, supersede the earlier, somewhat less accurate, results obtained in 1962 at essentially the same wavelength, and allow the mapping work (Sec. II-A) to proceed with the assurance that the effects of the mean surface slope on the reflectivity can be removed from the results.

TABLE II

RELATIVE ECHO POWER VS DELAY FOR THE MOON OBSERVED AT LINCOLN LABORATORY, M.I.T.

Delay (t) (μsec)	φ°	λ = 3.8 cm† (db)	λ = 23 cm† (db)	λ = 68 cm‡ (db)	Delay (t) (msec)	φ°	λ = 3.8 cm (db)	λ = 23 cm (db)	λ = 68 cm (db)
10	2.33	0	0	0	2.0	34.16	−12.5	−18.65	−21.3
20	3.37	− 0.6	− 0.85	− 0.6	2.25	36.30	−12.9	−19.1	−22.3
30	4.11	− 1.15	− 1.40	− 1.5	2.50	38.33	−13.35	−19.55	−22.7
40	4.77	− 1.55	− 1.9	− 2.2	2.75	40.28	−13.75	−19.85	−23.1
50	5.31	− 1.9	− 2.35	− 2.8	3.0	42.16	−14.05	−20.2	−23.5
60	5.83	− 2.2	− 2.75	− 3.3	3.25	43.97	−14.4	−20.5	−23.8
70	6.30	− 2.5	− 3.15	− 3.8	3.50	45.72	−14.7	−20.85	−24.1
80	6.73	− 2.75	− 3.55	− 4.3	3.75	47.42	−15.0	−21.15	−24.3
90	7.13	− 3.0	− 3.95	− 4.8	4.0	49.08	−15.3	−21.4	−24.5
100	7.53	− 3.2	− 4.3	− 5.2	4.25	50.69	−15.55	−21.7	−24.7
125	8.42	− 3.75	− 5.05	− 6.2	4.50	52.27	−15.8	−21.95	−24.9
150	9.22	− 4.2	− 5.8	− 7.0	4.75	53.82	−16.1	−22.35	−25.1
175	9.96	− 4.55	− 6.45	− 7.7	5.0	55.33	−16.3	−22.5	−25.35
200	10.65	− 4.9	− 7.0	− 8.4	5.25	56.82	−16.6	−22.75	−25.6
225	11.30	− 5.2	− 7.5	− 9.0	5.50	58.29	−16.9	−23.05	−25.9
250	11.92	− 5.5	− 8.0	− 9.7	5.75	59.72	−17.15	−23.3	−26.15
275	12.50	− 5.85	− 8.45	−10.15	6.0	60.95	−17.5	−23.6	−26.45
300	13.06	− 6.1	− 8.85	−10.7	6.25	62.55	−17.8	−23.85	−26.8
325	13.60	− 6.4	− 9.2	−11.1	6.50	63.93	−18.1	−24.2	−27.15
350	14.11	− 6.65	− 9.55	−11.6	6.75	65.36	−18.5	−24.55	−27.5
375	14.60	− 6.9	− 9.9	−11.9	7.0	66.65	−18.9	−24.95	−27.85
400	15.09	− 7.15	−10.2	−12.35	7.25	67.98	−19.3	−25.35	−28.25
425	15.56	− 7.4	−10.5	−12.7	7.50	69.31	−19.7	−25.8	−28.65
450	16.01	− 7.6	−10.8	−13.0	7.75	70.63	−20.2	−26.2	−29.0
475	16.45	− 7.8	−11.2	−13.3	8.0	71.94	−20.6	−26.65	−29.45
500	16.88	− 7.95	−11.35	−13.6	8.25	73.23	−21.05	−27.1	−29.95
600	18.51	− 8.5	−12.3	−14.6	8.50	74.53	−21.55	−27.6	−30.45
700	20.01	− 9.0	−13.2	−15.4	8.75	75.79	−22.05	−28.15	−30.95
800	21.40	− 9.4	−14.0	−16.2	9.0	77.06	−22.55	−28.7	−31.5
900	22.72	− 9.8	−14.6	−16.9	9.25	78.33	−23.15	−29.3	−32.1
1000	23.96	−10.1	−15.35	−17.6	9.50	79.59	−23.7	−29.95	−32.75
1100	25.16	−10.25	−15.95	−18.25	9.75	80.84	−24.5	−30.6	−33.35
1200	26.29	−10.75	−16.4	−18.9	10.0	82.09	−25.2	−31.35	−34.05
1300	27.39	−11.0	−16.8	−19.5	10.25	83.34	−26.1	−32.2	−34.9
1400	28.44	−11.25	−17.15	−20.0	10.50	84.58	−27.1	−33.25	−35.9
1500	29.42	−11.5	−17.45	−20.4	10.75	85.82	−28.5	−34.35	−36.9
					11.0	87.06	−30.0	−35.85	−38.35
					11.25	88.29	−31.2	−37.7	−40.1
					11.50	89.53	−32.0	−40.35	−42.7

† Pulse = 10 μsec; resolution at receiver = 10 μsec.

‡ Pulse = 12 μsec; resolution at receiver = 10 μsec.

II. WORK IN PROGRESS

A. HIGH-RESOLUTION 3.8-cm REFLECTIVITY MAPPING

1. Introduction

Considerable progress has been made in this reporting period toward obtaining 3.8-cm reflectivity maps of the lunar surface at a resolution of several kilometers. Prior to obtaining the final instrumentation at Haystack, emphasis has been placed on testing out all phases of the operating and data-reduction procedures. In the following sections, the tests carried out to date, together with the preliminary conclusions drawn from them, are first discussed. Second, the configuration and status of elements in the final "production" system are described.

2. System Tests

QPR (1966:2) gave a block diagram (p. 36) showing the data flow proposed for the 3.8-cm mapping program. In the current reporting period, we have attempted to assess the accuracy of the following portions of that program:

(a) The ephemeris, including most of the auxiliary calculations,

(b) The antenna pointing and Doppler tracking,

(c) The corrections to remove the effects of DC bias in the receiver phase detectors, of antenna beam shape, and of the mean lunar scattering law.

To this end, we have used an interim system configuration as shown in Fig. 13, where the numbers in parentheses indicate the computer (if any) involved in that element. The CDC 3200 and Univac 490 are in the same building as the Haystack radar; the SDS 9300 is located with the Craig/Fleck sequencer at the Millstone radar, about 2500 ft from Haystack. Measurements using the system to observe the moon were taken on 19 and 26 May and on 20, 22, 23, 25, and 26 July 1966.

The most serious limitation imposed by this interim configuration occurred in the use of the linear Doppler predictor. This device, originally built for another purpose, allowed one of the local oscillators in the multiple superheterodyne receiver to be slewed linearly to approximately match the rate of change of the Doppler frequency shift introduced by the moon.

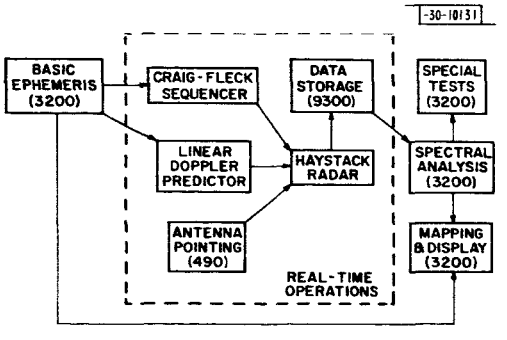

Fig. 13. Interim system configuration used to take 3.8-cm delay-Doppler mapping data.

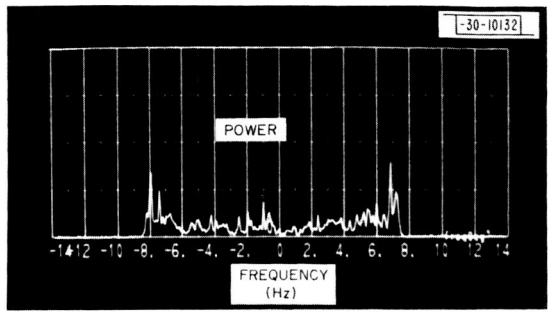

Fig. 14. Power spectrum of lunar echo originating 100 μsec behind leading edge. Duration of run was 2 min., and spectral resolution was 0.13 Hz. Note that mean frequency is displaced by about −0.5 Hz.

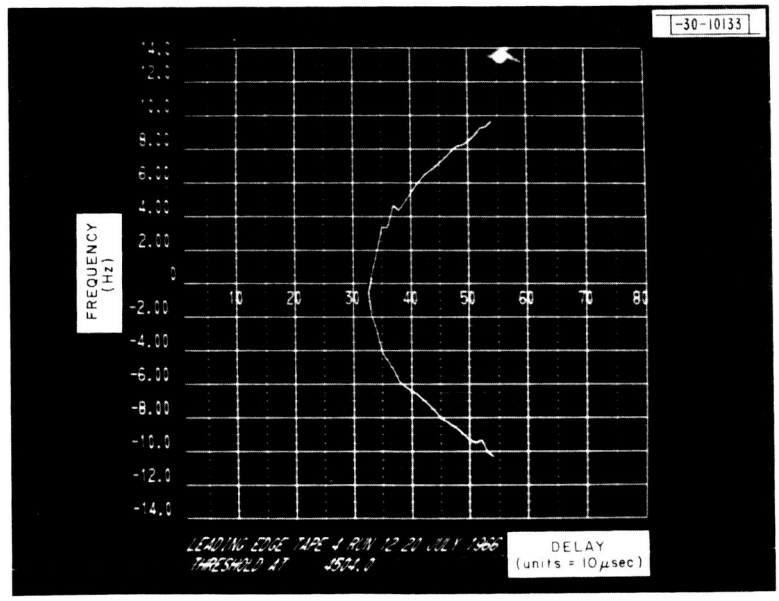

Fig. 15. Locus of positions of spectral power maxima in delay and frequency. "Nose" of curve (to left) represents position of earliest echo.

Since a resolution in frequency of the order of 0.13 Hz was sought, nonlinear terms (which vary over the course of the day) in the Doppler shift prevented the linear approximation from matching the actual received frequency to this accuracy for runs of duration in excess of from 2 to 5 min. A system is now nearly complete which will permit the local oscillator to be programmed to the necessary accuracy directly from the ephemeris, thereby eliminating this difficulty. For the tests carried out in the current reporting period, however, where statistical fluctuation in the amplitude was unimportant, the short duration of the runs presented no problem. The other serious limitation arose from difficulties in the transmitter pulsing apparatus which prevented use of peak powers in excess of about 50 kw. This problem – of no concern to the tests described here – will also be bypassed in the final configuration by the use of a different and more direct method.

In addition to the usual calibrations of system sensitivity and measurements of delay and frequency stability, a variety of tests involving lunar echoes were made. The first required recording and processing of echoes from the central portion of the lunar disk (the leading edge of the returned echo-power distribution). From these data, it was possible to check accurately the ephemeris predictions of signal delay and Doppler shift, and approximately the angular pointing. No difficulties were found in the pointing (which could be verified more accurately by other methods, in any case). However, small discrepancies in the predicted delay and Doppler shift were found.

Figure 14 shows an echo power spectrum obtained at a delay slightly later than the leading edge. The spectrum shows the characteristically sharp edges [see QPR (1966:1), pp. 44 – 50]; by averaging the frequencies corresponding to them, we were able to locate very accurately the frequency corresponding to echoes from the center of the lunar disk (and, therefore, presumably corresponding to the lunar center of mass). Data from several such spectra at different delays were compared to assess the accuracy of the approach, and it was concluded that the mean frequency could be determined with an error not exceeding the frequency resolution of 0.13 Hz.

When compared to the ephemeris, these measurements disclose discrepancies of up to about 1 Hz. Intensive effort has been applied to locate the source of these discrepancies. At the present time, there appear to be two possible explanations: (1) The hourly values of the lunar position supplied by the Naval Observatory are not tabulated to sufficient precision that their hourly differences (from which part of the apparent Doppler shift is obtained) maintain the necessary accuracy. This had been recognized previously, and in an attempt to minimize the resulting error a least-mean-squares fit to the data extending over several hours had been applied. There now appears to be some question as to whether this fit is being done optimally, and further improvements are being sought. (2) It is possible that the basic lunar orbit is not known with sufficient accuracy for the level of these current measurements. It is thought likely that both sources of error lie behind the Doppler discrepancies.

The observed delay has been obtained with considerable accuracy by the process illustrated in Fig. 15, where we see the locus of positions of maximum echo power density in delay and Doppler coordinates obtained from a series of spectra of the type shown in Fig. 14. By fitting an ellipse to this contour, the location of its "nose" may be obtained to an accuracy of a few microseconds. When this is done, discrepancies between the observed delay and the ephemeris are found which amount to about 20 μsec. It is felt that this error, as well as part of the Doppler

error discussed above, probably reflect inaccuracies in the theoretical statement of the lunar orbit. This problem will soon receive detailed attention; meanwhile, since the ephemeris errors are slowly varying in the course of an hour (they are tied to the monthly lunar orbit and not to the earth's rotation), they may be removed from the mapping by direct measurement in this manner just before and just after a run.

The second type of test measurement requires the observation of regions of the moon containing craters known to possess unusually large radar reflections. Based on information obtained from the Arecibo group (Thompson, 1965), the lunar craters Tycho, Copernicus, Aristarchus and Eratosthenes were examined in the May observations and, in addition, the craters Plinius, Bullialdus and Pytheas were examined in the July observations. The objective in these tests was to check all the details involved in the full mapping data reduction. By correlating the positions of small, highly reflective craters observed by radar with their positions as determined from optical photographs, it was hoped that it would be possible to establish confidence in the coordinate transformations. Also, by observing the variation in mean signal level in regions which appeared uniform optically, it was felt possible to check on the accuracy of correction which removed the effects of antenna angular directivity and the effects of the mean lunar surface scattering law. All of these hopes have been largely realized.

Figure 16 shows the results in delay-Doppler coordinates of a run taken 19 May on Copernicus. The enhanced reflectivity associated with the rim of this large crater may be clearly seen. As a test of detailed correlation in position, however, this crater is not as useful as the area surrounding Plinius. Figure 17 shows the transformation from delay-Doppler over to selenographic coordinates where the two grids have been properly superimposed according to calculations for one of the Plinius runs. In addition to accomplishing the coordinate transformation, the mapping program also removes the background system noise, and corrects for beam shape and for the lunar scattering law (which is assumed to be a function of delay only). It also has provision for normalizing the system gain and transmitter power, should these vary from run to run.

Figure 18 presents a contour plot of the results of the mapping program applied to a 5-min. run on Plinius taken on 20 July. A photograph of the corresponding area is given in Fig. 19. Both figures are labeled in lunar coordinates. Note that Plinius displays an extremely strong radar response – better shown in Fig. 20 – which is associated with the inside crater wall furthest from

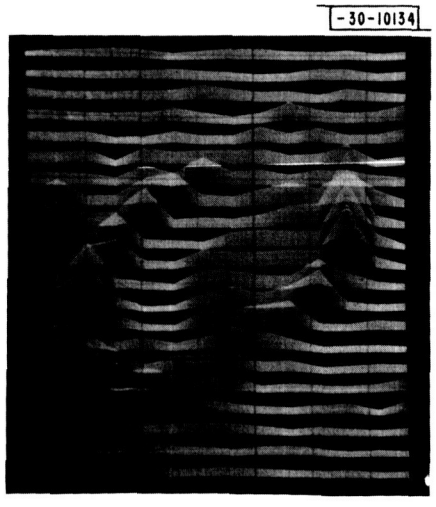

Fig. 16. Delay-Doppler map of radar reflectivity obtained at 3.8 cm from vicinity of Copernicus on 19 May 1966. Resolution here is 20 μsec in delay (corresponding to interval between successive spectra) and 0.25 Hz in frequency. Region of enhanced echoes appears to coincide roughly with walls of crater.

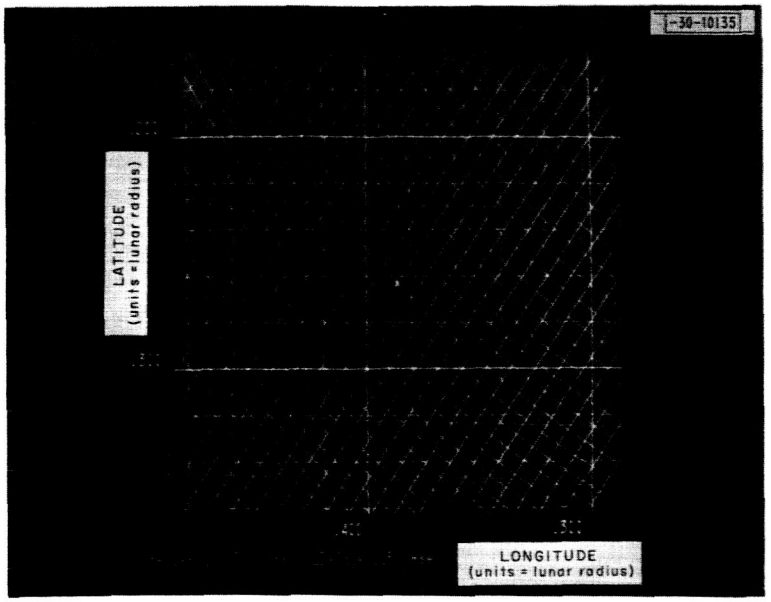

Fig. 17. Grid showing transformation from delay-Doppler to selenographic coordinates appropriate to Fig. 18. Plot is centered (as indicated) on optical location of center of crater Plinius. Contours of constant delay are separated by 50 μsec and are shown as portions of small circles running from upper left to lower right. Doppler contours are separated by 0.5 Hz and are sections of nearly straight lines running from upper right to lower left. Latitude and longitude are given in selenographic direction cosines.

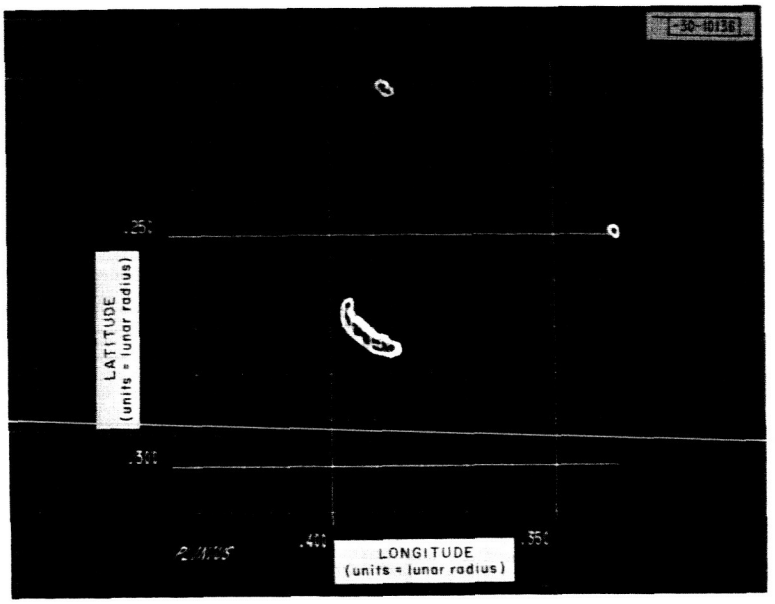

Fig. 18. Contour plot of selected levels of echo intensity obtained at 3.8 cm from vicinity of crater Plinius on 20 July 1966. Three regions of enhanced reflectivity may be seen which correlate well with positions of three crater walls most distant from radar as shown in Fig. 19.

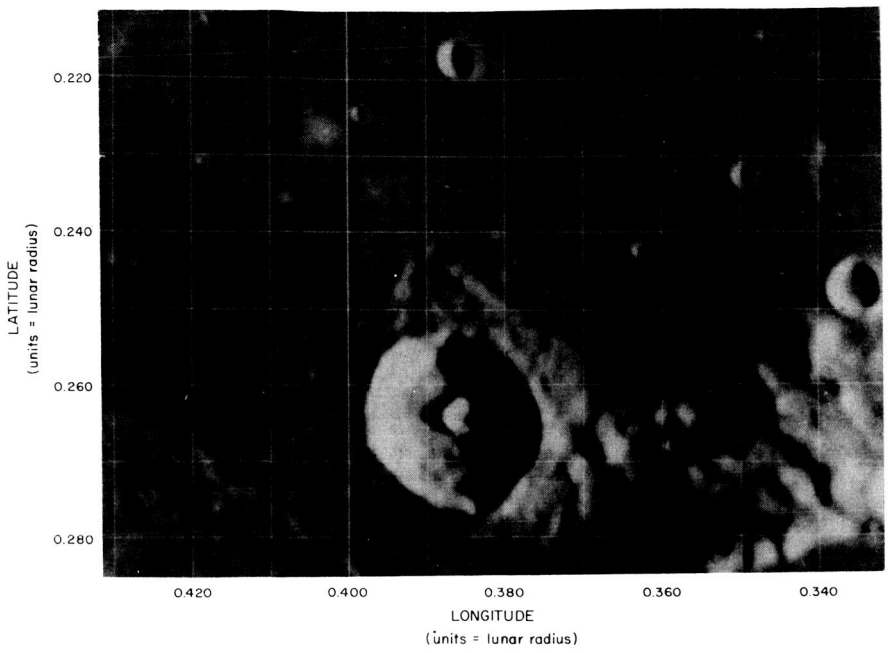

Fig. 19. Telescopic photograph of region of lunar surface in vicinity of Plinius (University of Chicago Lunar Atlas). Compare with radar data given in Fig. 18.

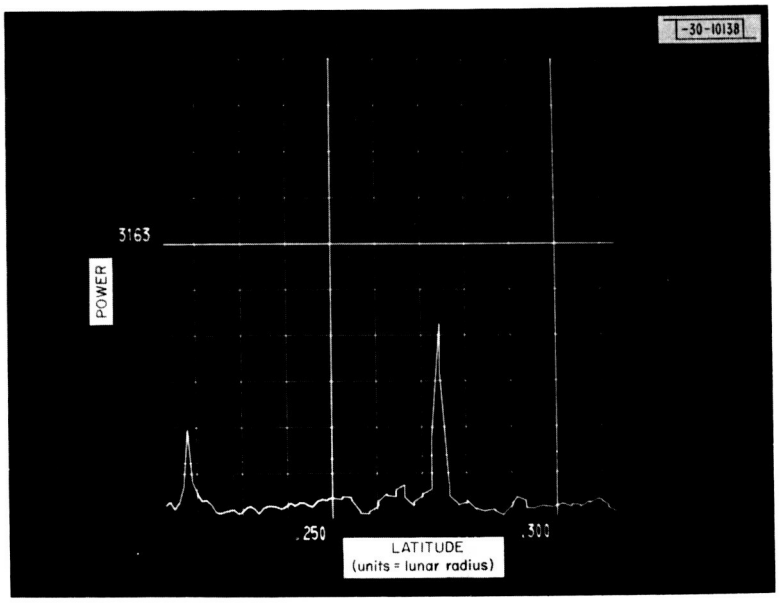

Fig. 20. Power profile drawn from data used in Fig. 18. Power density is shown (after reduction in mapping program) as function of selenographic latitude for selenographic longitude of 0.389. Thus, peak at left corresponds to top contour line on Fig. 18, and peak on right to portion of enhancement associated with Plinius. Lower-lying detail here is also probably significant.

the radar. In addition, lesser responses are seen which correlate well with some of the smaller craters in Fig. 19. In fact, the pattern of agreement between Figs. 18 and 19 is so good that there can be little doubt that the radar enhancements are indeed to be associated with the visible craters. The radar positions agree with the locations of the inside far walls in every case to approximately 2 km or better. It should be noted that a correction in delay and Doppler frequency, as given by an immediately preceding leading-edge run, has been applied in the reduction shown here.

Figure 20 shows a section through the plot of Fig. 18 where power density is given vs the latitude coordinate for constant longitude. The longitude has been chosen to include the strong response from Plinius and, in addition, shows the relatively uniform response from undifferentiated areas of the lunar surface which results following the corrections for beam shape and scattering law. From these results, we conclude that all corrections are apparently being applied correctly. A number of maps in the equatorial region have also been initiated but not yet fully reduced.

3. Status of Final System

The final system will differ from Fig. 13 in several respects. The Craig/Fleck sequencer located at Millstone will be replaced by a far more flexible design located adjacent to the control area at Haystack. This unit will provide for synchronization of transmission and reception using any desired pulse repetition rate, sampling of the received data in a wide choice of formats, calibration of the data, and automatic self-checking for a variety of errors. The Haystack radar sequencer is completed and is currently undergoing final checkout prior to integration into the Haystack radar system. It should be available after 1 September.

The linear Doppler predictor is being replaced by a direct link between the U490 computer and the frequency synthesizer which controls the local oscillator in one portion of the receiver. It will be able to adjust the receiver tuning so as to remove the Doppler frequency shift of the incoming signal to an accuracy of better than 0.1 Hz for a period as long as is desired. Implementation should be complete by 1 September.

Data storage, which is currently handled by the SDS 9300 computer at Millstone, will be possible both as it is organized now or, alternatively, using the CDC 3200 computer and its associated interface at Haystack. This flexibility should greatly increase the reliability of a specific scheduled operation since it provides a choice of two equally attractive methods.

One of the items of equipment which has proven most troublesome is the series-beam switch regulator (SBSR). To date, it has been impossible to operate at peak transmitted powers in excess of about 50 kw because of difficulties in this unit. Therefore, it has been decided to press strongly for the completion of a device using the modulating grids incorporated in the new generation of transmitting (klystron) tubes soon to be installed at Haystack. A number of advantages should stem from this decision: (a) The bulky SBSR unit will no longer be used; (b) operation using equipment in common with other programs of research will minimize setup time when shifting between experiments; and (c) a peak power of at least 500 kw should become available with the new equipment. This latter figure is some ten times the power currently available for the lunar mapping program and should greatly improve the measurements made at large relative delays where signals are quite weak with the current system. It is hoped that the use of these new transmitting tubes for this program may be possible by late October.

B. PROGRESS ON 8-mm RADAR

The radar employing the 10-watt transmitter has been put into operation. All parts of it were checked out individually in June, and on 30 June an attempt at lunar observation was made. The attempt failed, but the failure seemed to be ascribable to a single cause: when loaded by the antenna, the klystron was pulled to a frequency different from that of the oscillator used as reference in the phase-lock system. The test was encouraging in that nearly everything performed perfectly. The shift in frequency of the klystron was subsequently accommodated by merely changing the frequency of the reference oscillator and allowing it a few days to stabilize. Because of vacation absences, it was necessary to postpone until August a second attempt to make radar contact with the moon. There has been continuing progress, however, in supplying or refining parts of the system that are not essential for making radar contact but that must be present when quantitative data on reflectivity are being recorded.

The 10-watt system is the first stage in a four-stage program. The succeeding stages are: increase transmitter power to 50 watts; provide polarization diversity for transmitted signal and install a two-polarization receiving and recording system; and increase transmitter power to 1000 watts.

The increase of power from 10 to 50 watts will require only some small changes in the transmitter. The polarization diversity makes necessary a whole new RF head, presently under construction. Initial planning called for this RF head to employ the 1000-watt tube. Because of administrative delays in the contract approval for the kilowatt tube, polarization effects must be studied in an interim way while awaiting development of that tube. Since the moon is expected to behave like a rather rough object at 35 GHz, it is expected that the echo will exhibit a considerable degree of depolarization, and that the weaker polarization component can probably be measured (with low accuracy) with a transmitted power of 50 watts.

Increasing the transmitted power to 1000 watts will entail a new power supply, a closed pure-water cooling system, extensive changes in the RF plumbing, and a new source of stable 35 GHz. The power supply has been procured, and bids for the cooling system are in hand. The critical items of plumbing are the 1-kw hybrid and the 500-watt phase shifter that are necessary for controlling the polarization of the transmitted wave; it appears that these items, though novel, are procurable. The 1000-watt tube will be an amplifier klystron, which will be preferable to the system now in use, in which a 10- or 50-watt klystron oscillator is phase-locked to a crystal oscillator through the mediation of a frequency multiplier and a phase comparator. The new tube will simply amplify a 35-GHz signal derived by multiplication from a crystal oscillator; elimination of the phase-locking system is expected to improve the reliability and the stability of the transmitter. A further advantage of the new system is that the frequency will be set once and for all by the crystal oscillator; consequently, the 1000-watt tube can be driven by an oscillator of the highest quality, with consequent improvement in the sharpness of the spectrum, whereas in the old system the frequency is determined by the transmitter tube, and every time the tube is replaced by a new one (or even when its frequency is altered by a change in the load, as happened on 30 June) the frequency of the reference oscillator has to be changed. Actually, the improvement in spectrum is a necessity if the benefits of high power are to be fully realized.

The need for a high-quality 35-GHz source has posed the most serious problem in the design of the high-power transmitter – apart, of course, from the construction of the klystron itself, which represents an advance in the klystron art. The preferred operating frequency for a highly stable crystal oscillator is about 5 MHz. Converting this frequency to 35 GHz involves multiplying the frequency by 7000, and this operation inevitably multiplies any frequency or phase modulation by 7000, thus raising its level by 77 db. If one allows another 3 db for noise introduced by the multiplier, then, in order to achieve a signal-to-noise ratio of 20 db at the input to the klystron amplifier, one must start with a crystal oscillator at which the noise due to frequency or phase modulation is at least 100 db below the signal. An alternative is to multiply, for example, from a 70-MHz oscillator that is stabilized by locking to the 5-MHz standard. In effect, the 70-MHz oscillator reduces the noise by acting as a very narrow filter for the signal originating at 5 MHz; therefore, the noise level at the output of the 5-MHz oscillator is less critical.

The 5-MHz frequency standard that is part of the 35-GHz radar has been modified, in the expectation that it can yield the signal-to-noise ratio of 100 db that multiplication by 7000 demands. A vendor has been found who has undertaken the exacting task of building a multiplier chain for converting 5 MHz to 35 GHz. As insurance against possible disappointment, the multiplier is being built so that the first stages of the chain can be replaced by a locked oscillator, in the event that the signal-to-noise ratio after direct multiplication by 7000 is not good enough. Since this scheme involves locking one oscillator to another, it partakes of the disadvantages of the low-power system now in use and, if possible, it will be avoided.

III. NOTES ON FUTURE WORK

A. UNAMBIGUOUS COHERENT RADAR MAPPING

1. Introduction

When the moon is observed with an antenna whose polar diagram is wider than the angular extent of the moon, there is a twofold ambiguity in the range-Doppler mapping technique [see QPR (1966:1)]. This ambiguity can be removed by using a narrow-beam antenna, such as the Haystack antenna operated at 3.8 cm. Since it is of considerable interest to be able to map the moon unambiguously and to study the polarization properties of features at 23 as well as at 3.8 cm, some consideration has been given to the possibilities for mapping without having to rely on the beam resolution. Ideas for such procedures are not new and have been suggested before (Thomson, 1965), but the ideas do not seem to have been carried out in practice. The mapping technique to be outlined below does not have to depend on range resolution at all, and might thus be of interest in radar systems not having a range-resolution capability.

2. Description of Mapping Method

It is well known (see Bracewell, 1962) that the observation of a two-dimensional complex correlation function over a plane normal to the direction of an extended radio source will provide information on the two-dimensional distribution of power over the source. In fact, the power distribution over the source is given by

$$W(S_1, S_2) = \text{const} \iint \rho(x, y) \exp[-(2\pi i/\lambda)(S_1 x + S_2 y)]\, dx\, dy \qquad (20)$$

where S_1 and S_2 are angular offsets along orthogonal directions from the center of the source, λ is the wavelength, and $\rho(x, y)$ is the two-dimensional complex spatial correlation function of the fields at the point of observation. Hence, it is sufficient to measure the two-dimensional correlation function for all different spacings and directions in order to derive the angular power distribution of the source.

In radar observations of the moon and, to a limited extent, the planets, it is possible to make use of an analogous principle. The relative rotation of the object and the observer causes the diffraction pattern to drift over the receiving antenna without altering its form. The autocorrelation function of the signal at the receiver can, therefore, be interpreted as a spatial correlation function provided the speed and direction of drift of the diffraction pattern is known. In order for a complete correlation function to be constructed, it is necessary that the direction of drift of the diffraction pattern goes through an angle of 180°. Only in the case of the moon is this condition fulfilled. When the direction of drift does not change appreciably, only a single frequency spectrum – or a single "strip-distribution" of the source – can be obtained. A two-dimensional distribution of power over the source can thus only be obtained provided additional assumptions are made. One assumption may be a source which is circularly symmetric. Analysis of lunar frequency spectra on this assumption has been carried out and the known power-range distributions have been reproduced to within about 2 db.

The proper two-dimensional mapping procedure can be carried out in the following steps. Collect a number M of frequency spectra:

$$W(f_\ell, \varphi_m)$$

where

$\ell = 1 \rightarrow N$

N = number of filters

$m = 1 \rightarrow M$

φ_m = angle between true lunar axis (projected) and libration axis for run m.

An estimate of the weighted correlation function for run m is

$$R_W(\tau, \varphi_m) = \sum_{\ell=1}^{N} W(f_\ell, \varphi_m) \exp[-2\pi i \tau (f_\ell - f_{om})] \tag{21}$$

where f_{om} is the Doppler frequency offset of the feature we are interested in during run m, and

$$f_\ell = \ell \cdot \Delta f \quad . \tag{22}$$

Note that $R_W(\tau, \varphi_m)$ is periodic in τ with period $\tau_P = 1/\Delta f$. The correlation function should, therefore, <u>not</u> be estimated from Eq. (21) for $\tau > \tau_{max} = \frac{1}{2}\Delta f^{-1}$.

Since the procedure used in computing the frequency spectra $W(f_\ell, \varphi_m)$ implies a triangular weighting of the correlation function, we should "unweight" Eq. (21) by a ramp function:

$$R_{est}(\tau, \varphi_m) = \frac{1}{1 - |2\tau| \cdot \Delta f} \sum_{\ell=1}^{N} W(\ell \cdot \Delta f, \varphi_m) \exp[-2\pi i (\ell \Delta f - f_{om})\tau] \quad . \tag{23}$$

Since the limb-to-limb Doppler shift is varying from run-to-run, we normalize so that they all have the same equivalent width by introducing

$$\Theta = \tau \cdot f_{Lm} \tag{24}$$

where f_{Lm} is the center-to-limb Doppler offset for run m. It is obtained

$$R_{est}(\Theta, \varphi_m) = \frac{1}{1 - |2\Theta| \cdot \Delta f / f_{Lm}} \sum_{\ell=1}^{N} W(\ell \Delta f, \varphi_m) \cdot \exp[-2\pi i \Theta (\ell \Delta f - f_{om})/f_{Lm}] \quad . \tag{25}$$

In order to reduce noise in the final map, it is necessary to filter the data by applying a ramp function which is narrower than the original ramp:

$$R_f = \frac{1 - \text{Filt} \cdot |\Theta|}{1 - 2|\Theta| \Delta f / f_{Lm}} \sum_{\ell=1}^{N} W(\ell \Delta f, \varphi_m) \exp[-2\pi i \Theta (\ell \Delta f - f_{om})/f_{Lm}] \tag{26}$$

where the filtering factor must satisfy

$$\text{Filt} > 2\Delta f/f_{Lm} \quad .$$

With this estimate of $R_f(\Theta, \varphi_m)$ available, formula (2) may be used to compute the two-dimensional distribution of power over the lunar disk area of interest:

$$P(\xi, \eta) = \int_0^{1/\text{Filt}} \Theta d\Theta \int_0^{2\pi} d\varphi_m \frac{1 - \text{Filt} \cdot |\Theta|}{1 - 2|\Theta| \Delta f/f_{Lm}} \cdot \sum_{\ell=1}^{N} W(\ell \Delta f, \varphi_m)$$

$$\cdot \exp[-2\pi i \Theta(\ell \Delta f - f_{om})/f_{Lm}] \cdot \exp[2\pi i \Theta(\xi \cos\varphi_m + \eta \sin\varphi_m)$$

$$= \int_0^{1/\text{Filt}} \Theta d\Theta \int_0^{\pi} d\varphi_m \{\text{Re}(R_f) \cos[2\pi\Theta(\xi \cos\varphi_m + \eta \sin\varphi_m)]$$

$$-\text{Im}(R_f) \sin[2\pi\Theta(\xi \cos\varphi_m + \eta \sin\varphi_m)]\} \quad . \qquad (27)$$

Certain difficulties do arise with the method due to the presence of a specular component which does not move with the surface. This may, however, be overcome by gating out the initial pulse from the moon where this is possible, or by observing in depolarized radiation where the specular return is strongly suppressed.

This method will shortly be tested out on moon echoes obtained with the Millstone radar at 23 cm. If the method works well, it will be used in conjunction with polarization observations to study various lunar surface features. The results of these tests will be reported in a future Quarterly Progress Report.

ACKNOWLEDGMENTS

The work of most of the technical personnel of Group 31, Surveillance Techniques, which operates the facilities of the Field Station, in preparing and conducting the work reported to date is gratefully acknowledged, as is the work of members of Group 46, Microwave Components, in cooperating with Dr. McCue on the 8.6-mm radar.

The use of the facilities of the Lincoln Laboratory Millstone-Haystack complex, provided by the U.S. Air Force, is also gratefully acknowledged.

APPENDIX A

Let an arbitrary pair of two-dimensional orthogonal unit vectors be given in terms of $\vec{e}_x$ and $\vec{e}_y$ by

$$\vec{e}_1 = \alpha\vec{e}_x + \beta\vec{e}_y$$

$$\vec{e}_2 = -\beta^*\vec{e}_x + \alpha^*\vec{e}_y \quad . \tag{A-1}$$

The components of the complex field along these directions are

$$E_1 = (\vec{e}_1 \cdot \vec{E})$$

$$E_2 = (\vec{e}_2 \cdot \vec{E}) \quad . \tag{A-2}$$

The difference in the power in these two orthogonal modes is

$$\langle|E_1|^2\rangle - \langle|E_2|^2\rangle = S_2(|\alpha|^2 - |\beta|^2) + S_3(\alpha\beta^* + \alpha^*\beta) + S_4(\alpha\beta^* - \alpha^*\beta)(-i) \quad . \tag{A-3}$$

By Schwartz inequality,

$$[\langle|E_1|^2\rangle - \langle|E_2|^2\rangle]^2 \leqslant (S_2^2 + S_3^2 + S_4^2)(|\alpha|^2 + |\beta|^2)^2 \quad . \tag{A-4}$$

But from Eq.(A-1) it follows that $|\alpha|^2 + |\beta|^2 = 1$, and the well-known definition of degree of polarization Eq.(3) is therefore seen to be physically reasonable.

APPENDIX B

Rotation of the coordinate system through an angle ψ causes the components of a vector $\vec{E}$ to transform according to the rule

$$\begin{Bmatrix} E_{x\psi} \\ E_{y\psi} \end{Bmatrix} = \begin{Bmatrix} \cos\psi & \sin\psi \\ -\sin\psi & \cos\psi \end{Bmatrix} \begin{Bmatrix} E_x \\ E_y \end{Bmatrix} . \tag{B-1}$$

The corresponding transformation of the Stokes vector can be found by simple substitution to be

$$\begin{Bmatrix} S_{1\psi} \\ S_{2\psi} \\ S_{3\psi} \\ S_{4\psi} \end{Bmatrix} = \begin{Bmatrix} 1 & 0 & 0 & 0 \\ 0 & \cos 2\psi & \cos 2\psi & 0 \\ 0 & -\sin 2\psi & \cos 2\psi & 0 \\ 0 & 0 & 0 & 1 \end{Bmatrix} \begin{Bmatrix} S_1 \\ S_2 \\ S_3 \\ S_4 \end{Bmatrix} \tag{B-2}$$

or abbreviated

$$\vec{S}_\psi = T\vec{S} . \tag{B-3}$$

The Mueller matrix in the rotated coordinate system is

$$M_\psi = TM\tilde{T} \tag{B-4}$$

where $\tilde{T}$ is the transpose of T. Measuring ψ relative to the plane of incidence of the scattering element, we obtain, in general,

$$M_\psi = \begin{Bmatrix} M_{11}^o & M_{12}^o \cos 2\psi & -M_{12}^o \sin 2\psi & 0 \\ M_{12}^o \cos 2\psi & M_{22}^o \cos^2 2\psi + M_{33}^o \sin^2 2\psi & (M_{33}^o - M_{22}^o) \sin 2\psi \cos^2\psi & 0 \\ -M_{12}^o \sin 2\psi & (M_{33}^o - M_{22}^o) \sin 2\psi \cos 2\psi & M_{33}^o \cos^2 2\psi + M_{22}^o \sin^2 2\psi & 0 \\ 0 & 0 & 0 & M_{44}^o \end{Bmatrix} . \tag{B-5}$$

REFERENCES

Beckmann, P., "Radar Backscatter from the Surface of the Moon," J. Geophys. Research 70, 2345-2350 (1965a).

_____, "Shadowing of Random Rough Surfaces," IEEE Trans. Antennas Propag. AP-13, 384-388 (1965b).

Beckmann, P., and Klemperer, W. K., "Interpretation of the Angular Dependence of Backscattering from the Moon and Venus," J. Research Natl. Bur. Standards 69D, 1669-1677 (1965).

Beckmann, P., and Spizzichino, A., The Scattering of Electromagnetic Waves from Rough Surfaces (Macmillan, New York, 1963).

Born, M., and Wolf, W., Principles of Optics (Pergamon Press, New York, 1959).

Bracewell, R. W., "Radio Astronomy Techniques," in Handbuch der Physik, Vol. LIV (Springer-Verlag, Berlin, 1962), pp. 42-129.

Daniels, F. B., "Radar Determination of the Root Mean Square Slope of the Lunar Surface," J. Geophys. Research 68, 449-453 (1963).

Davis, J. R., and Rohlfs, D. C., "Lunar Radio-Reflection Properties at Decameter Wavelengths," J. Geophys. Research 69, 3257-3262 (1964).

Evans, J. V., "Radio-Echo Observations of the Moon at 3.6-cm Wavelength," Technical Report 256, Lincoln Laboratory, M.I.T. (19 February 1962), DDC 274669.

Evans, J. V., and Hagfors, T., "On the Interpretation of Radar Reflections from the Moon," Icarus 3, 151-160 (1964).

_____, "Radio Echo Studies of the Moon at 23 cm. Wavelength," accepted for publication in J. Geophys. Research (1966).

Evans, J. V., and Pettengill, G. H., "The Radar Cross-Section of the Moon," J. Geophys. Research 68, 5098-5099 (1963a).

_____, "The Scattering Behavior of the Moon at Wavelengths of 3.6, 68 and 784 Centimeters," J. Geophys. Research 68, 423-447 (1963b).

Hagfors, T., "Some Properties of Radio Waves Reflected from the Moon and Their Relation to the Lunar Surface," J. Geophys. Research 66, 777-785 (1961).

Hagfors, T., Brockelman, R. A., Danforth, H. H., Hanson, L. B., and Hyde, G. M., "Tenuous Surface Layer on the Moon: Evidence Derived from Radar Observations," Science 150, 1153-1156 (1965).

Peake, W. P., "The Interaction of Electromagnetic Waves with Some Natural Surfaces," Report 898-2, Ohio State University Research Foundation (30 May 1959).

Pettengill, G. H., and Henry, J. C., "Enhancement of Radar Reflectivity Associated with the Lunar Crater Tycho," J. Geophys. Research 67, 4881-4885 (1962).

Rea, R. D., Hetherington, N., and Mifflin, R., "The Analysis of Radar Echoes from the Moon," J. Geophys. Research 69, 5217-5223 (1964).

Rice, S. O., "Reflection of Electromagnetic Waves from Slightly Rough Surfaces," in The Theory of Electromagnetic Waves (Interscience, New York, 1951), pp. 351-378.

Rumsey, V. H., "The Reaction Concept in Electromagnetic Theory," Phys. Rev. 94, 1483-1491 (1954).

Thompson, T. W., "Lunar Mapping by Coherent Pulse Analysis," Radio Science 69D, 1667-1669 (1965).

Thomson, J. H., private communication (1965).